Received: 2 August 2021 | Revised: 5 April 2022 | Accepted: 25 April 2022

IET Renewable Power Generation

DOI: 10.1049/rpg2.12496

The Institution of Engineering and Technology WILEY

ORIGINAL RESEARCH

Experimental assessment and validation of inertial behaviour of virtual synchronous machines

Md Asif Uddin Khan[1] | **Qiteng Hong**[1] | **Di Liu**[1] | **Agusti Egea-Àlvarez**[1] | **Andreas Avras**[2] | **Adam Dyśko**[1] | **Campbell Booth**[1] | **Djaved Rostom**[3]

[1]Department of Electronic and Electrical Engineering, University of Strathclyde, Glasgow, UK

[2]Power Networks and Demonstration Centre (PNDC), University of Strathclyde, Glasgow, UK

[3]Network Operability, National Grid ESO, Faraday House, Warwick Technology Park, Warwick, UK

Correspondence
Qiteng Hong, Postal: Level 4, Technology and Innovation Centre (TIC), University of Strathclyde, 99 George Street, Glasgow, G1 1RD, UK.
Email: q.hong@strath.ac.uk

Md Asif Uddin Khan, Department of Electronic and Electrical Engineering, University of Strathclyde, Glasgow, UK.
Email: asif.u.khan@strath.ac.uk

Funding information
This work is jointly funded by the National Grid ESO and EPSRC RESUE Project (EP/T021829/1) in the UK

Abstract

Increasing integration of converter-interfaced renewable generation has led to significant operational challenges for power systems. Such challenges are mainly caused by the different capabilities and dynamic responses of the converters compared with synchronous machines, for example, converters do not naturally provide inertia to the system. Virtual Synchronous Machine (VSM) is considered as a promising solution to address the challenges associated with reduced system inertia via the provision of emulated inertial response to support the operation of converter-dominated power systems. However, it has been observed that the dynamic behaviour of the VSM could differ significantly from that of a Synchronous Condenser (SC) and a Synchronous Generator (SG) in terms of inertial response provision, even when the VSM is configured with the same inertia constant. Furthermore, effective practical methods for evaluating the damping performance of VSMs are not presently available. To gain a better understanding and achieve a more accurate assessment of the dynamic inertial and damping performance of VSMs, this paper presents an experimental methodology for systematic evaluation of the dynamic response of the VSM in the frequency domain using the Network Frequency Perturbation (NFP) method. Experimental design and implementation of the NFP method are presented to assess VSM system's equivalent inertia and damping constants, where the VSM system under test can be treated as a black box without any knowledge of internal settings and control design. Case studies are conducted, where the proposed experimental design has been applied for testing and assessing the inertial and damping constants of a physical 246 kVA VSM prototype driven by a Battery Energy Storage System with comparison of the SC and SG with equivalent inertia constant. Power-Hardware-in-the-Loop (PHiL) testing is also conducted to demonstrate the VSM's inertia performance. The studies demonstrate that the developed experimental approach based on NFP method provides a valuable tool for network operators and manufacturers for evaluating the inertial and damping performance.

1 | INTRODUCTION

The operation of conventional power systems largely relies on the inherent properties of synchronous generators (SGs), which provide inertia, damping and fault current capacity to facilitate the system's protection and control. In recent decades, there has been a significant increase in renewable generation replacing conventional SGs and this trend is expected to continue in the coming years [1]. Typically, renewable sources require power electronics-based converters to interface with the AC power networks. The dynamic behaviour of these types of power electronics devices is significantly different from conventional SGs and is largely dependent upon their controllers [2]. One of the most typical control strategies for converter-based resources is to provide constant power to the grid, which does not naturally provide inertia and frequency support to the system.

Furthermore, due to the constraint of the current capacity of the semiconductor switches, their capability of providing large fault currents is very limited [3, 4]. As a result, the overall short circuit level (SCL) and inertia of the system are decreasing dramatically and the system strength is becoming progressively weaker with the rapid increase of non-synchronous generation in the power system. In the GB power system, it is anticipated that by 2025, the inertia level can decrease by 40% [5] and the minimum SCL in some regions can decrease by over 80% [6]. In addition to fault level and inertia contribution, the capability of converters to remain connected to the system during severe faults or other disturbances is also very crucial. Furthermore, converters' general responses to such events need to be fully understood and evaluated for reliable operation of future power systems that either will be fully powered by or will be mostly dominated by power-electronics based converters. To address the aforementioned operational challenges caused by the increasing penetration of converter-interfaced generation, two key approaches are being widely investigated as the solution: one is to install synchronous condensers (SCs) to mitigate the effect of decommissioned SGs; the other is to enable converters with grid forming capability, to provide inertial response, fast frequency regulation and fault current injection, all of which can contribute to more secure and stable system operation.

SC is a type of synchronous machine without a prime mover, so it does not provide any sustained active power to the network but can supply and absorb (if necessary) reactive power to/from the system to stabilise the grid voltage. Therefore, SCs are conventionally used for power factor correction and voltage regulation [7]. Due to the similar inherent behaviour and construction as SGs, SCs are considered to have a critical role in supporting the operation of systems dominated by converters [8, 9]. SC is a very mature solution widely used in power systems worldwide, and in recent years, there has been an increasing trend of using this technology to solve the challenges in weak power systems, for example, countries like the UK, Denmark and USA have all deployed SCs in their network in recent years to support the integration of renewable resources [10–12]. A major positive aspect of the SC is that, unlike converters, its inertial and fault current support to the system are inherent, so it does not require dedicated measurements to provide such services. Furthermore, it may be possible to reuse the decommissioned SGs by converting them into SCs, since the implementation of both machines is very similar. In the GB transmission system, as part of the Stability Path-finder initiative raised by the transmission system operator [13], inertia has been considered as a service provided to the system and some in-service SGs start to run as SCs in certain periods (e.g., Cruachan power station) to provide inertia support to the system [14]. However, since large amount of SGs are being decommissioned, potentially there is a need for significant newly-installed or converted SCs to be online to fully compensate the impact of increasingly decommissioned SGs.

Another approach being widely investigated is to control the converters as VSMs, thus providing properties that could be offered by SGs. The key benefit of this approach is that there will be a significant increase of converter capacity in the system anyway, and new control with synthetic inertia support could be deployed in newly installed converter units. Also, there is an opportunity to enable such capability in the existing converters, potentially via updating the software/firmware. Reference [15] suggests the concept of VSM, which aims to replicate the behaviour of SGs via the deployment of specifically designed controllers on converters. VSM is a type of grid forming converter and if implemented properly, it can maintain voltage and frequency of the grid in a similar manner to an SG. In the literature, there are different types of implementations of VSM [16–18]. Through the provision of emulated inertia from VSMs, it is expected that by 2025, the inertia of the GB power system will be increased from 115 GVAs to an equivalent inertia level of 175 GVAs and it is possible to further achieve an equivalent inertial level of 270 GVAs (which is approximately the maximum inertia level in today's GB system) [19].

The previous work reported in [20] presented a detailed analysis of several technical criteria to test the capability of the VSM to meet the minimum requirements as defined by National Grid ESO Stability Pathfinder [13] and compared the VSM performance with a Synchronous Condenser (SC) and a Synchronous Generator (SG) under short-circuit faults, severe frequency deviations and voltage depression events. It was found that the VSM is capable of providing a set of desirable properties via the proper design of the control in providing valuable service to support the future grid operation. Specifically, the VSM can provide emulated inertia response at a similar time scale as the SG and SC, thus providing effective inertia support to the system.

Despite extensive work has been conducted to understand and assess the dynamic performance and capability of VSMs in support the grid operation, it has been observed that the dynamic behaviour of the VSM could differ significantly from that of an SC and an SG in terms of inertial response provision, even when the VSM is configured with the same inertia constant. This could introduce significant challenges for the network operators when assessing the performance of the VSMs against the expected or required inertial behaviour, thus leading to the difficulties in wider application of the technology in the system. Furthermore, effective methods for evaluating the damping performance of VSMs are not presently available.

Therefore, as an extension to the authors' work in [20] and in order to gain a better understanding and achieve a more accurate assessment of the dynamic inertial and damping performance of VSMs, this paper presents a new experimental design and implementation for the assessment of the dynamic behaviour of a VSM in terms of inertia response provision and its damping performance based on the frequency domain-based Network Frequency Perturbation (NFP) method.

The NFP method was originally proposed in [21] as a tool for assessing the instantaneous penetration level of the converter-based generation in GB power system via investigating the generator response to an enforced change in network frequency. The work gives a theoretical foundation for estimating different parameters of the generation unit and provides a unique insight into the dynamics of a generator as it allows to make a clear

verification of the inertia support of the generator. However, to the authors' best knowledge, there is no publication so far with a methodology to design the experimental procedure and setup for implementing the NFP method, and use it for the purpose of assessing and evaluating the inertial and damping performance of VSMs, thus presenting a clear major gap for manufacturers and network operators for adopting the methods for VSM testing.

To address the gap, this paper presents the design and implementation of an experimental environment procedure that realise the NFP methods for assessing the dynamic inertia and damping response of physical VSM units. Case studies are conducted, where the proposed experimental design has been applied for testing and assessing the inertial and damping constants of a physical 246 kVA VSM prototype driven by a Battery Energy Storage System (BESS) with comparison of the SC and SG with equivalent inertia constant. Power-Hardware-in-the-Loop (PHiL) testing using a 540 kVA Triphase unit and a reduced GB transmission network model in a Real-Time Digital Simulator (RTDS) is also conducted to demonstrate the VSM's inertia performance and dynamic interaction with other sources in the power system.

The rest of the paper is organised as follows: Section 2 presents the analyses of the dynamic performance of the VSM in terms of inertia response provision as compared to SC and SG, and describes the challenge of assessing frequency response from the VSM; Section 3 illustrates the NFP method that can determine the inertia constant and damping factor of the generation units in a comprehensive manner; Section 4 presents and explains the experimental implementation of the NFP method along with experimental PHiL setup, and the physical test results that validate the inertia constant and damping factor of the VSM unit estimated through NFP method; and finally, Section 5 concludes the paper with a summary of outcomes observed from the physical tests.

2 | INERTIA RESPONSE OF VSM, SG AND SC

As mentioned earlier, paper [20] presents simulation results and several technical criteria to evaluate the dynamic performance and capabilities of the VSMs as compared to SCs and SGs.

One of the ways of verifying inertial response of a generating unit is through the application of system frequency ramp. This type of test can give an indication whether the inertial response is present, and the amount of inertial power response being generated. In [20], two frequency ramps with a RoCoF magnitude of ±1 Hz/s were simulated, where the positive ramp of 2 s duration was applied, followed by the negative ramp of 5 s, as shown in the top graph of Figure 1. The covered frequency range is between 47 and 52 Hz, as stipulated in [13]. The output power from the machines, due to imposed frequency ramps, can be observed in the bottom graph of Figure 1.

Three different generating technologies were simulated, that are, VSM, SG and SC. It is important to state in this regard that inertia constant for all three units is set as $H = 2$ s, and the theoretical values of delivered power by the generation units due to constant frequency ramp (RoCoF) can be calculated through (1), where, H is the inertia constant, S is the rated apparent power of the generation unit, f_0 is the system frequency before a frequency event, and ΔP is the active power increment resulting from the frequency ramp with a constant value of RoCoF.

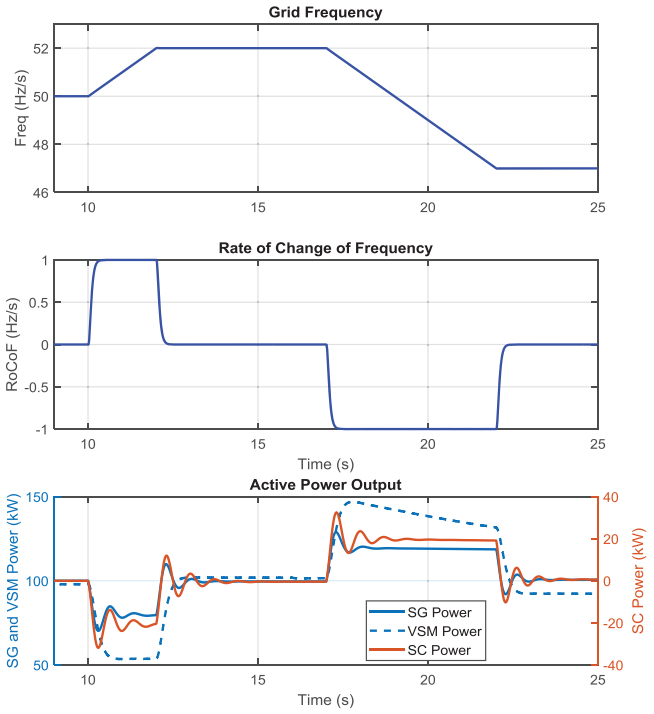

FIGURE 1 Inertia response to frequency ramps

$$\Delta P = -\frac{2 \cdot H \cdot S \cdot RoCoF}{f_0} \tag{1}$$

It is necessary to state that when a small VSM (or SG/SC) is connected to a large power system (i.e., frequency is completely dominated by the system), the relatively small machine does not have any obvious impact on the frequency. However, if a unit under test behaves according to the standard swing equation representing a synchronous machine (SM), when a frequency ramp with fixed RoCoF value is applied (using a strong controllable voltage source on the grid side), power change by the generating unit can be estimated using (1). In an ideal case, the inertia response of VSM and SM should be similar for the same value of inertia constant.

It can be observed from Figure 1 that VSM is capable of contributing fast inertia power, which is comparable with the SC and SG. However, the magnitude of inertia power output from the VSM differs significantly from both of the SC and SG, that is, higher power is produced initially, which subsequently decreases with time, even though the RoCoF value remains constant.

The comparison between assumed and expected active power increments are presented in Table 1, where, ΔP_{est} presents the active power change estimated using (1), and ΔP_{act} presents the

TABLE 1 Comparison of inertial power response to a frequency ramp with constant RoCoF

Solution	H (s)	S (kVA)	ΔP_{est} (kW)	ΔP_{act} (kW)	Error (%)
SG	2	246	19.75	20	1.25
SC				20	1.25
VSM				38	48

actual change of active power when frequency ramp with fixed value of RoCoF is applied in simulation (or laboratory testing). The value of ΔP_{act} is established by subtracting initial active power output of the generation unit from the measured steady-state active power level during frequency ramp event (refer to Figure 1). The error between theoretical and measured active power changes is calculated using (2). To compare the VSM response with the SG and SC, the error definition (2) has been used.

$$Error = \left| \frac{\Delta P_{act} - \Delta P_{est}}{\Delta P_{est}} \right| \times 100\% \tag{2}$$

As can be seen in Table 1, the inertia constant, rated apparent power, RoCoF and frequency value for all three machines are the same, hence the expected theoretical estimated power for all three generation units is also the same. However, while the errors between the calculated and observed power for the SG and SC are low (i.e., around 1.25%), the error is observed to be 48% for the VSM unit in this test.

One potential reason for the difference could be the different implementation of inertia and/or damping characteristics of the VSM unit. Commercial VSMs are generally presented as a "black box" to the network and system operator. As demonstrated in this case, it is possible that with the typical configuration value of inertia coefficient, VSM might behave differently from what is expected. This could be problematic from the network operators' perspective since inertial behaviour is typically characterised by the swing equation of the conventional SG and it will be ideal if VSMs' inertial response could be adapted to the existing methods of system stability analysis, that is, the conventional definition of the generator parameters is preferable as it is well understood in theory and operational practice.

Therefore, it is necessary to have effective experimental methods for assessing and evaluating equivalent value of the inertia constant and damping coefficient of the VSM in order to have an accurate understanding of its anticipated performance. This is particularly important when rolling out the technology for wider application in the network.

3 | NETWORK FREQUENCY PERTURBATION (NFP) METHOD

Dynamic linear systems can be represented and characterised by transfer functions and illustrated by Bode or Nyquist plots. The NFP method originally proposed in [21] is based on the same approach where an intentional perturbation on system frequency is applied either in simulation through controllable voltage source, or in the laboratory using a grid emulator. The source frequency is modulated following the value determined by (3).

$$f(t) = f_0 + \Delta f \cos\left(2\pi f_{NFP_{mod}} t\right) \tag{3}$$

where f_0 is the system nominal frequency, Δf is the magnitude of the frequency change, and $f_{NFP_{mod}}$ is the frequency of the applied modulation in Hz. For simplicity the amplitude of the disturbance is kept constant at $\Delta f = 0.5$ Hz (but this is not a requirement and could be reduced if needed, especially around the resonant frequency, if the amplitude of the observed power oscillation is too high, for example, power oscillation reaching the generator rating).

The generating unit directly connected to such a source will respond to the frequency change with modulated active power which can be described by (4).

$$P_{out}(t) = P_{ref} + \Delta P \cos\left(2\pi f_{NFP_{mod}} t + \phi_{\Delta P}\right) \tag{4}$$

By varying frequency of the modulation, the power response (P_{out}) from the generating unit is recorded, and through Fourier analysis both amplitude (ΔP) and phase angle ($\phi_{\Delta P}$) of the resulting power perturbation can be derived. It is assumed that the input signal perturbation amplitude (Δf) is sufficiently small, and therefore, the system can be treated as linear. Any linear system perturbed with a single frequency will produce a response with the same frequency, with a certain magnitude of ΔP and phase angle of $\phi_{\Delta P}$. The perturbance amplitude is assumed as $\Delta f = 0.5$ Hz (i.e., 1% of nominal frequency). The practical value of perturbance amplitude depends on the expected peak response around the resonant frequency (typically 1–3 Hz). This forms a response characteristic R as shown in (5), defined as a ratio of power response (output) to frequency perturbation (input).

$$R = \frac{\Delta P \angle \phi_{\Delta P}}{\frac{\Delta f}{f_0}} \tag{5}$$

The dynamic behaviour of a standard SM, governed by the second order swing equation, can be illustrated through the block diagram shown in Figure 2. Although the exact implementation of a power electronic converter can be different, the overall design of the VSM controller is based on the same swing equation, and therefore, can be represented by a second order transfer function as shown in (6), where, K_X is the inverse of the impedance between VSM's internal voltage source (i.e., equivalent emf) and the connection point with the grid, H is the inertia constant and D is the damping factor. By comparing (6) with an ideal second order function, the natural frequency (ω_n) and damping ratio (ζ) can also be determined as shown in

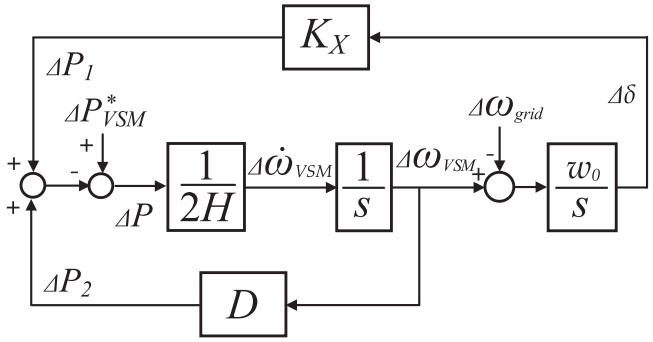

FIGURE 2 Generic synchronous machine model implemented in a VSM

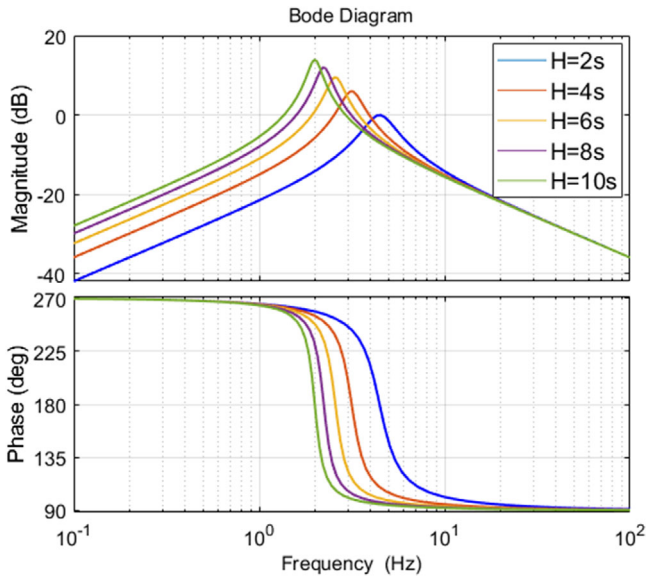

FIGURE 3 Impact of inertia constant on frequency characteristic

Equations (7) and (8).

$$\frac{\Delta P}{\Delta\omega_{grid}} = \frac{-K_X s}{s^2 + \frac{D}{2H}s + \frac{K_X\omega_0}{2H}} \tag{6}$$

$$\omega_n = \sqrt{\frac{K_X\omega_0}{2H}} \tag{7}$$

$$\zeta = \frac{D}{4}\sqrt{\frac{2}{HK_X\omega_0}} \tag{8}$$

Using the simplified SM model as shown in Figure 2, examples of bode plot characteristics for different values of H and D can be produced and are presented in Figures 3 and 4. It can be observed from Figure 3, the peak positions and slope of the bode plot change with the value of inertia constant (H). However, with the variation in damping factor (D), the sharpness and peak of the amplitude characteristic change as can be observed in Figure 4.

The experimental implementation of the NFP method requires a voltage source with sufficient power rating to perturb

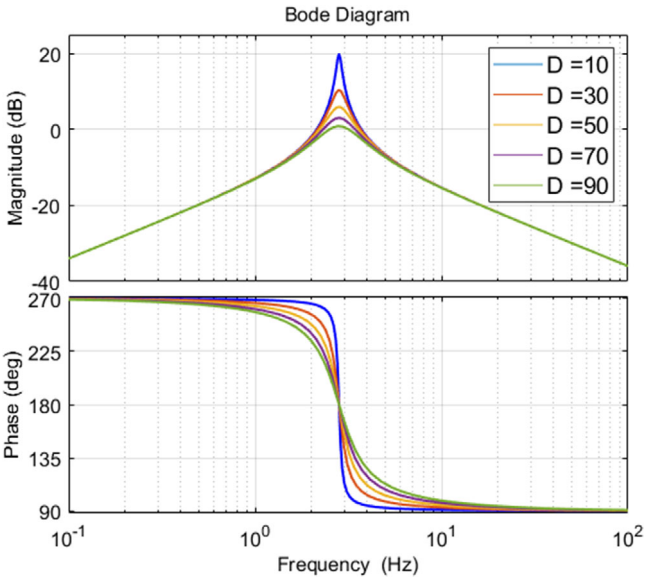

FIGURE 4 Impact of damping factor on frequency characteristic

frequency on the terminals of the device under test according to (3). From the captured frequency response characteristic R, the values of inertia constant (H) and damping factor (D) can be derived. There are a few alternative approaches to achieve this, as described in the following subsections.

3.1 | Transfer function curve fitting

The parameters (i.e., H, D and K_X) of the generating unit can be obtained through the curve fitting approach, where the known amplitude response shown in (9), derived from the transfer function (6) for $s = j\omega$, is fitted into the measured amplitude characteristic points using least square method, where H, D, and K_X are the curve fitting parameters.

$$|G(j\omega)| = \left|\frac{\Delta P}{\Delta\omega_{grid}}\right| = \left|\frac{-j\omega K_x}{-\omega^2 + j\omega\frac{D}{2H} + \frac{K_x\omega_0}{2H}}\right| \tag{9}$$

Additional advantage of this approach is that the value of K_x, which depends on the reactance between the generator internal voltage and the test source internal voltage, does not need to be known in order to estimate inertia and damping parameters.

3.2 | Asymptote at low frequency

Since the inertia constant value has an impact on the slope height of the bode plot's magnitude characteristic at low frequency and can be described in the asymptote, R_H as shown in Equation (10), which is derived from (9). The dominant factor in the denominator of (9) reduces to $\frac{K_X\omega_0}{2H}$ for very small value of ω and then can be simplified as (10) by only considering the magnitude of the equation. A point at low-frequency

range (on the linear part of the magnitude characteristic) must be selected to calculate the slope (i.e., R_H and $f_{NFP_{mod}}$) at the low frequency region of the bode plot and by rearranging the (10), inertia constant (H) can be estimated. However, using this approach damping factor (D) cannot be determined.

$$R_H = 2H\left(\frac{f_{NFP_{mod}}}{f_0}\right) \tag{10}$$

3.3 | Peak response

To estimate the value of H and D using (7) and (8), firstly the values of ω_n and ζ need to be determined from the bode plot. The frequency corresponds to the peak of the bode plot indicates the natural frequency (ω_n) of the generation unit. Assuming the value of K_X is known, inertia constant of the machine can be calculated using (7), where ω_0 is the system frequency (e.g., typical value is 314.16 rad/s for a 50 Hz system).

In order to obtain the damping factor (D), the shape around the amplitude peak response can be used. The damping ratio (ζ) is related to the damping quality factor which can be determined through (11). Furthermore, the damping quality factor (Q) can be determined through natural frequency and cut-off frequencies as shown in Equation (12). As explained earlier the natural frequency (ω_n or f_n) is the frequency corresponds to the peak of the bode plot. The cut-off frequencies (f_1 and f_2) are the frequencies corresponding to the points with magnitudes that are 3 dB below the peak response point of the bode plot. Subsequently, damping factor can be determined through rearranging (8).

$$\zeta = \frac{1}{2Q} \tag{11}$$

$$Q = \frac{f_n}{f_2 - f_1} \tag{12}$$

4 | DESIGN OF THE EXPERIMENTAL SETUP AND IMPLEMENTATION BASED ON NFP AND CASE STUDIES

4.1 | Experimental implementation of the NFP test

The experimental setup for the NFP test configuration used for estimating the inertia constant and damping of the VSM unit is shown in Figure 5. The configuration uses a grid emulator composed of a Triphase programmable bi-directional power converter [22] rated at 540 kVA. The RTDS controls the voltage at the terminal of the Triphase unit that is connected to the tested physical VSM unit. The VSM unit consists of a BESS, a 246 kVA inverter with VSM control and an isolation transformer. The detailed specifications of the VSM unit and the isolated transformer are presented in Tables 2 and 3, respectively.

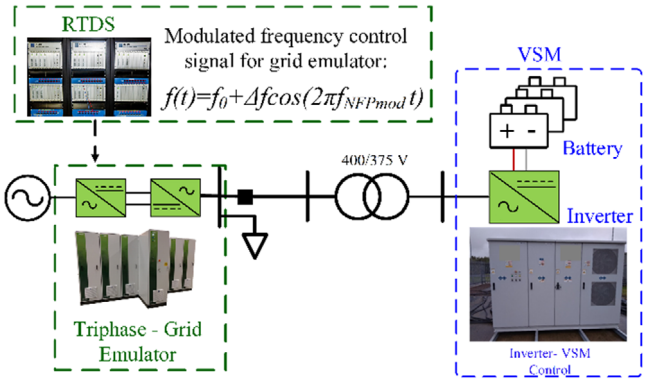

FIGURE 5 Experimental laboratory setup for NFP test

TABLE 2 Parameters of the VSM under test

Parameter	Value	Description
$V_{DC_{min}}$	1091.2 V	Minimum dc voltage
$V_{DC_{max}}$	1443.2 V	Maximum dc voltage
$V_{DC_{nom}}$	1300 V	Nominal dc Voltage
$I_{DC_{max}}$	156 A	Absolute maximum dc current for operation
$P_{DC_{max}}$	170 kW	For 0% state of charge (1091.2 V)
$V_{VSM_{nom}}$	375 V	Nominal voltage at the ac side of VSM
$I_{VSM_{max}}$	380 A	Maximum current at the ac side of VSM
$S_{VSM_{nom}}$	246.82 kVA	Nominal apparent power of VSM
f_{nom}	50 Hz	Nominal frequency

TABLE 3 Electrical parameters of isolation transformer

Parameter	MV side	LV side
Rated Power	700–1000 kVA	1000 kVA
Nominal voltage	371.2–550 V	405 V
Nominal current	1049.73–1088.75 A	1425.56 A
Tap changer	No	No
Connection Type	D	Yn
Frequency	50 Hz	
Vector group	Dyn11	
Impedance value at 75°C	5%	±10%
No load losses	1.5 kW	±15%
Load losses at 75°C	12 kW	±15%
Total losses	13.5 kW	±10%

To remove any noise and unwanted signals from the measurements, second order low pass filters have been used in post processing of the simulation results. The filtering of the harmonic frequencies did not pose any significant challenge as those frequencies were sufficiently distant from the analysed frequency range between 0.02 Hz and approximately 10 Hz.

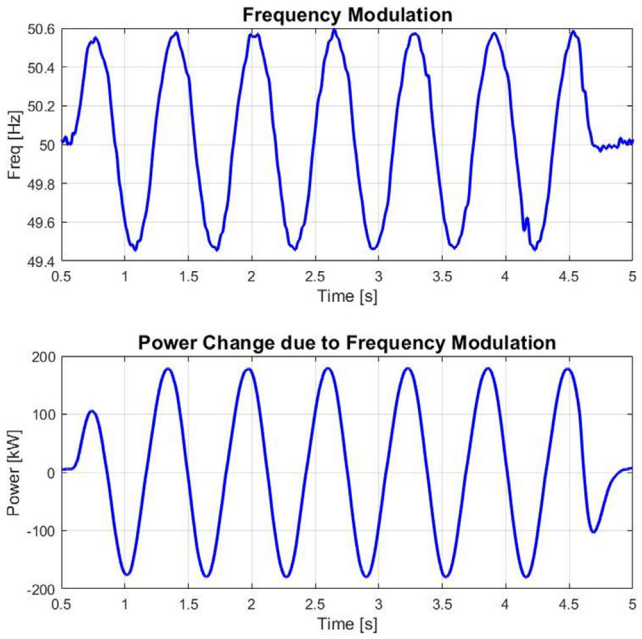

FIGURE 6 Power output under frequency modulation during the NFP test

To carry out the NFP test as explained in Section 3, the following procedure needs to conducted through RTDS laboratory setup:

- The 3-phase voltage source is programmed in RTDS with its frequency defined as (3), where $f_{NFP_{mod}}$ is varied from 0.02 Hz to 20 Hz. During this test, it is ensured that the voltage magnitude is maintained at the nominal value at all times so that the relation between active power and frequency can be analysed.
- At any given value of $f_{NFP_{mod}}$ the VSM outputs are captured, that are, frequency, RoCoF, voltage, current and power supplied by the VSM. The only difference is that during the NFP test, the collection of data during a steady-state condition required a sufficiently long time, that is, at least one (preferably two) cycles of the modulation frequency. The modulation frequency is changed from 0.02 Hz to 20 Hz. To achieve a reasonably accurate representation of the characteristic, approximately 10 tests have been performed per decade, that is, 30 tests within 3 decades.
- The power output of the VSM unit with one of the time-domain simulations for the modulated frequency is presented in Figure 6 as an example. The output power is then analysed using Fourier Transform to determine the amplitude of the VSM's frequency response. A bode plot for amplitude is plotted by setting $f_{NFP_{mod}}$ on the x-axis and amplitude on the y-axis.

While in this work the NFP test has been conducted on a physical system, the same process was also set up and applied to an SC and an SG with the same rating and inertia constant with the VSM in simulation for comparison.

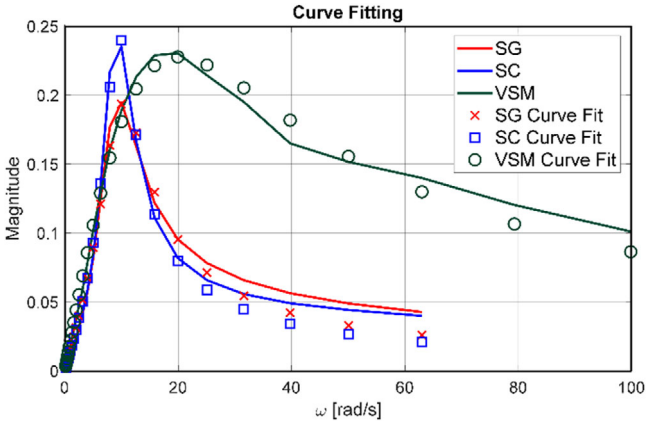

FIGURE 7 Estimating H, D and K_X through curve fitting approach

TABLE 4 Estimated values of H, D and K_X using curve fitting approach

Generating Unit	H (s)	D	K_X
SG	2.408	39.86	1.606
SC	2.282	24.42	1.305
VSM	3.517	276.6	8.959

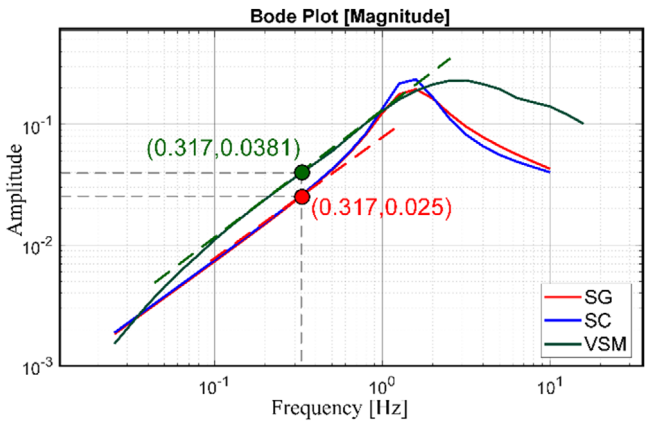

FIGURE 8 Estimation of the inertia constant H using the asymptote at low frequency

4.1.1 | Curve fitting approach

The least square curve fitting method has been applied to the measured amplitude characteristic points to obtain the approximated characteristic (9) (as described in Section 3.1). The resulting curve fitting graphs are plotted in Figure 7. The estimated values of the parameters H, D and K_X for all three generating units, are presented in Table 4.

4.1.2 | Asymptote at low-frequency range

The magnitude characteristics for all three units are shown in Figure 8. As can be seen from the figure, at low frequency, SC

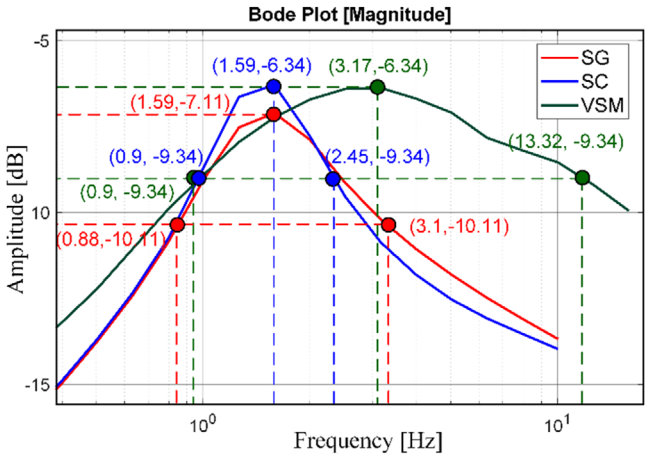

FIGURE 9 Estimation of the inertia constant H and damping factor D using magnitude peak response

TABLE 5 Estimated values of H and D using peak response approach

Generating Unit	H (s)	D
SG	2.53	70.51
SC	2.05	40
VSM	3.55	553.65

and SG plots are superimposed, and hence, according to the asymptote approach, inertia constant for both SC and SG will be the same. A point at the low-frequency range as shown in Figure 8 has been selected on the linear part of the slope. Finally, (10) has been rearranged to calculate the value of the inertia constant and that provides the value H equates to 3 s for VSM, and for SC and SG, the calculated inertia constant (H) is 1.97 s.

4.1.3 | Peak response

The magnitude bode plots in dB with for all three units are shown Figure 9. From this figure, natural frequency and cut-off frequencies for three generation units are measured. Using the Equations (7), (8), (11) and (12), the value of H and D estimated and presented in Table 5.

It is necessary to mention that as the phase characteristics are not used in the experimental derivation of H and D, they are not presented in Figures 7–9 (unlike Figures 3 and 4, examples of both magnitude and phase characteristics obtained from the known transfer function (6) with assumed values of H and D). The assumed and estimated values of H and D for the VSM units using the three approaches are summarised in Table 6. From this table it can be seen that the assumed H and D value are 2 s and 256 respectively. However, from the NFP tests, the estimated value H varies between 3 and 3.55 s and estimated D are 553.65 for peak response and 276.6 for curve fitting approach.

As mentioned in Section 2, the inertial response of the VSM unit could be significantly different from the conventional SG and SC even though the value of inertia constant is same. It can be seen from the NFP test that the VSM's setting for H in this test case is lower than the effective equivalent H. To verify the inertia constant of the VSM estimated through NFP test, the frequency ramp test has been carried out using a physical VSM model. Furthermore, an additional laboratory test has been carried out and discussed in Section 4.3, to demonstrate the VSM's capability to limit the RoCoF in the low inertia power system.

TABLE 6 Estimated H and D for the VSM unit through NFP test

Method	Assumed H	Estimated H	Assumed D	Estimated D
Curve fitting	2 s	3.517 s	256	276.6
Asymptote at low frequency	2 s	3 s	256	–
Peak response	2 s	3.55 s	256	553.65

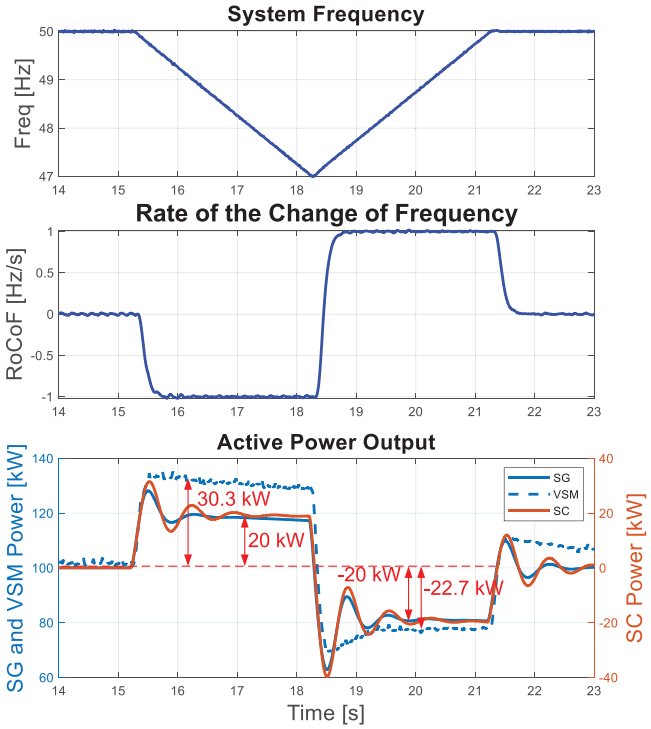

FIGURE 10 Experimental results (frequency, RoCoF and active power output from VSM) for a frequency ramp with inertia constant of 2 s

4.2 | Frequency ramp tests

To further verify the NFP tests results, a frequency ramp test has been carried out for the VSM in the laboratory setup as shown in Figure 5. To carry out the frequency ramp tests, the grid emulator controlled by RTDS is programmed for frequency ramp instead of frequency perturbation. The results are presented in Figure 10, where the inertia constant (H) for all three machines is configured as 2 s.

As it can be seen from Figure 10, a constant RoCoF of −1 Hz/s is applied at around 15.2 s for a duration of 3 s. As a result, the frequency of the system decreases to 47 Hz at around 18.2 s, and during this negative RoCoF, the VSM unit provides an inertial power of approximately 30.3 kW. However, according to calculation (1), the expected inertia power should be 19.75 kW. Therefore, this suggests the VSM provides 53.42% additional inertia power than the expected values. The same frequency ramp test has been carried out in simulation for the SG and SC units of the same rating and inertia constant, and it can be seen from Figure 10, the power change is reasonably close to the expected value. From the NFP method outcome presented in Section 4.1, the inertia constant (H) of the VSM was estimated to be equal to or higher than 3 s, while the converter was configured with $H = 2$ s. Using (1) with $H = 3$ s, expected change of power is 29.619 kW, which is close to the power change observed in Figure 10. The error between observed power change and calculated change in this case is only 1.89% showing experimental consistency between the NFP and the ramp methods, thus demonstrating that the NFP method could accurately assess the VSM's inertial response.

During the second part of the test a constant RoCoF of +1 Hz/s is applied and the frequency returns to 50 Hz. As a result, a decrease in active power can be observed, and according to the results, the VSM unit provides a negative active power of −22.7 kW while according to formula (1), the expected inertia power from an equivalent SG should be −19.75 kW. Therefore, again an additional negative active power response of 14.94% from the VSM due to positive RoCoF can be observed. However, this time the change of power is lower than the one observed during the negative RoCoF. Assuming the value of $H = 3$ s (as obtained from the NFP test), the estimated change of power due to RoCoF of +1 Hz/s should be −29.619 kW. The error between expected and estimated power change is 23.36% in this case. This result highlights the fact that the power response from a VSM may not be fully symmetrical, that is, the power may change differently depending on whether frequency is increasing or decreasing (in this test 30.3 kW for ramping down, and −22.7 kW for ramping up).

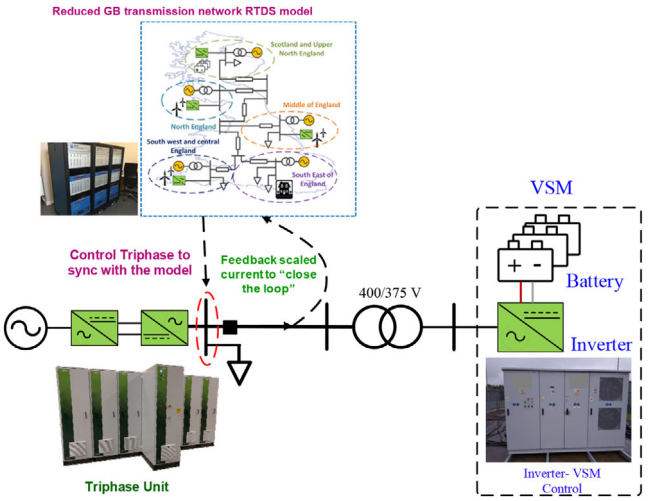

FIGURE 11 Experimental setup for PHiL simulation

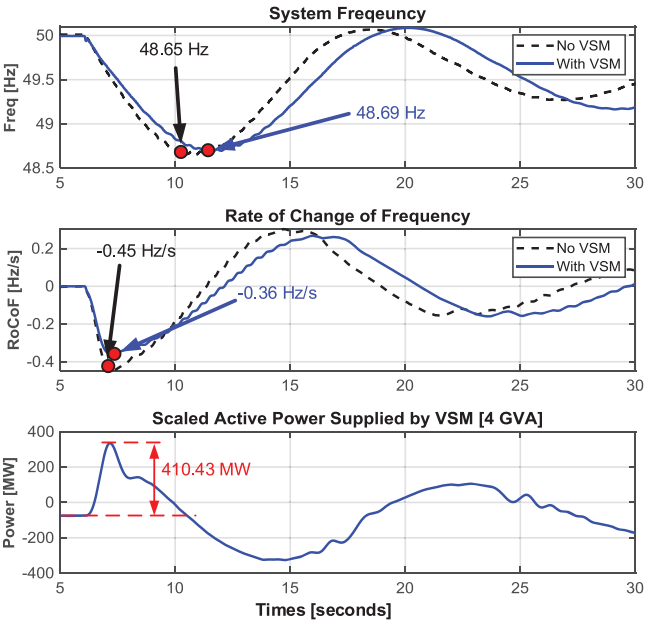

FIGURE 12 Experimental results (frequency, RoCoF and active power output from VSM) for a frequency disturbance with 1.8 GW generation loss

4.3 | Testing of the effectiveness of VSM inertial response to support the system frequency stability using PHiL setup

The experimental setup for the PHiL simulation is shown in Figure 11. The Triphase is controlled with a voltage signal from a reduced GB transmission network model which is running in the RTDS environment, and the feedback current is scaled to close the loop (as shown in Figure 11) so that the inertia response from the VSM can be scaled and reflected in the simulation.

It is essential to study and analyse the VSM capability to support GB power system under varying inertia levels and power imbalance scenarios. To perform such tests, the reduced GB transmission network model has been configured to emulate 95 GVAs inertia level. In this case, a test has been conducted by simulating a large frequency disturbance caused by sudden load-generation imbalance of 1.8 GW (the largest single loss of generation being considered in GB network) with the VSM under test. The inertia constant (H) of the VSM is set to 8 s. For comparison purposes a reference case without any support from the VSM unit has also been simulated. By comparing frequency profile of these two tests, the VSM capability of limiting system RoCoF can be assessed. By limiting RoCoF unwanted loss of main (LoM) protection operation can be avoided.

The results of this test are shown in Figure 12. As can be seen, during "No VSM" case, there is no active power contribution from the VSM and as a result, due to loss of 1.8 GW active power, a frequency dip of 48.65 Hz with a RoCoF of

–0.45 Hz/s has been observed. In the case with VSM, the VSM unit with physical capacity of 246.82 kVA is scaled up to 4 GVA in the simulation via PHiL setup. Therefore, the overall inertia of the system is increased by 32 GVAs (or 33.68%) with the emulated inertia from the VSM. As can be seen from the results in Figure 12, the system RoCoF improves from –0.45 Hz/s to –0.36 Hz/s (i.e., 20% improvement) due to a large inertial power support of 410.97 MW from the VSM unit in the RTDS. However, it has been observed that the frequency of the system with VSM still decreases to 48.69 Hz; therefore, the connection of VSM unit does not provide significant improvement in terms of frequency nadir during the frequency disturbance. This suggests that the emulated inertia can potentially be an effective option in limiting the system RoCoF, but it provides limited benefit in mitigating frequency nadir as it does not provide sustained power to the system.

5 | CONCLUSIONS

It is known that VSMs are capable of providing effective inertial response, thus representing a promising solution for addressing the challenges associated with rapidly decreasing system inertia due to the increasing penetration of converter-based renewable generation. However, the behaviour of the VSM units can differ significantly from the conventional SC and SG depending on the specific design and implementation. This introduces significant challenges for network operators to assess and validate the actual performance of the VSMs against the expected or required inertial behaviour.

To address this gap, the paper presents an experimental methodology for systematic evaluation of the dynamic response of VSMs in frequency domain using the NFP method. The method enables better understanding and more accurate assessment of the dynamic inertial and damping performance of VSMs. The VSM unit under test can be treated as a black box without any knowledge of internal settings or control design, which is highly desirable for practical applications. The laboratory test results are presented, where the proposed experimental design was applied for assessing the inertial and damping constants of a physical 246 kVA VSM prototype driven by a BESS. The tested VSM unit was then compared with the SC and SG with equivalent inertia constant.

Additionally, PHiL type testing was also conducted to demonstrate the VSM's inertia performance in a larger power system context. The studies demonstrates that the developed experimental approach based on NFP method provides a valuable tool for network operators and manufacturers for experimentally evaluating the inertial and damping performance.

CONFLICT OF INTEREST

The authors have no conflicts of interest to this work.

PERMISSION TO REPRODUCE MATERIALS FROM OTHER SOURCES

None

DATA AVAILABILITY STATEMENT

The data that support the findings of this study are available on request from the corresponding author. The data are not publicly available due to privacy or ethical restrictions.

REFERENCES

1. National Grid: Future Energy Scenarios Navigation, pp. 1–124. National Grid, London (2020)
2. Shuai, Z., Shen, C., Yin, X., Liu, X., Shen, Z.J.: Fault Analysis of inverter-interfaced distributed generators with different control schemes. IEEE Trans. Power Deliv. 33(3), 1223–1235 (2018). https://doi.org/10.1109/TPWRD.2017.2717388
3. Khan, M.A.U., Hong, Q., Dysko, A., Booth, C.: Performance analysis of the overcurrent protection for the renewable distributed generation dominated microgrids. In: IEEE Region 10 Symposium 2020. IEEE, Piscataway (2020)
4. Khan, M.A.U., Hong, Q., Dysko, A., Booth, C., Wang, B., Dong, X.: Evaluation of fault characteristics in microgrids dominated by inverter-based distributed generators with different control strategies. In: 8th International Conference on Advanced Power System Automation and Protection. IEEE, Piscataway (2019)
5. National Grid ESO: Operating a Low Inertia System (2020)
6. National Grid: System Operability Framework 2016 (2016)
7. Oliver, J.A., Ware, B.J., Carruth, R.C.: 345 MVA Fully water-cooled synchronous condenser for dumont station part i. application considerations. IEEE Trans. Power Appar. Syst. PAS-90(6), 2758–2764 (1971). https://doi.org/10.1109/TPAS.1971.292972
8. Teleke, S., Abdulahovic, T., Thiringer, T., Svensson, J.: Dynamic performance comparison of synchronous condenser and SVC. IEEE Trans. Power Deliv. 23(3), 1606–1612 (2008). https://doi.org/10.1109/TPWRD.2007.916109
9. Tzelepis, D., Hong, Q., Booth, C., Papadopoulos, P.N., Ramachandran, J., Yang, G.: Enhancing short-circuit level and dynamic reactive power exchange in Gb transmission networks under low inertia scenarios. In: 2019 International Conference on Smart Energy Systems and Technologies (SEST). IEEE, Piscataway (2019). https://doi.org/10.1109/SEST.2019.8849020
10. Jia, J., Yang, G., Nielsen, A.H., Gevorgian, V.: Investigation on the combined effect of VSC-based sources and synchronous condensers under grid unbalanced faults. IEEE Trans. Power Deliv. 34(5), 1898–1905 (2019) https://doi.org/10.1109/TPWRD.2019.2914342
11. Zhou, G., et al.: Synchronous condenser applications: Under significant resource portfolio changes. IEEE Power Energy Mag. 17(4), 35–46 (2019) https://doi.org/10.1109/MPE.2019.2909005
12. Hume, C.: Phoenix: Project Progress Report 2020 (2020). https://www.spenergynetworks.co.uk/userfiles/file/Phoenix_PPR_2020_External.pdf
13. National Grid ESO: Stability Pathfinder RFI Technical Performance and Assessment Criteria (2019). https://www.nationalgrideso.com/document/148341/download
14. OFGEM: Phoenix: System security and synchronous compensators (2016)
15. Nguyen, H.T., Yang, G., Nielsen, A.H., Jensen, P.H.: Combination of synchronous condenser and synthetic inertia for frequency stability enhancement in low-inertia systems. IEEE Trans. Sustain. Energy. 10(3), 997–1005 (2019). https://doi.org/10.1109/TSTE.2018.2856938
16. Du, C., Bollen, M.H.J., Agneholm, E., Sannino, A.: A new control strategy of a VSC-HVDC system for high-quality supply of industrial plants. IEEE Trans. Power Deliv. 22(4), 2386–2394 (2007). https://doi.org/10.1109/TPWRD.2007.899622
17. Zhang, L., Harnefors, L., Nee, H.P.: Modeling and control of VSC-HVDC links connected to island systems. IEEE Trans. Power Syst. 26(2), 783–793 (2011). https://doi.org/10.1109/TPWRS.2010.2070085
18. Silva, B., Moreira, C.L., Seca, L., Phulpin, Y., Lopes, J.A.P.: Provision of inertial and primary frequency control services using offshore multiterminal HVDC networks. IEEE Trans. Sustain. Energy 3(4), 800–808 (2012). https://doi.org/10.1109/TSTE.2012.2199774

19. Zhu, J., Booth, C.D., Adam, G.P., Roscoe, A.J., Bright, C.G.: Inertia emulation control strategy for VSC-HVDC transmission systems. IEEE Trans. Power Syst. 28(2), 1277–1287 (2013). https://doi.org/10.1109/TPWRS.2012.2213101
20. Khan, M.A.U., et al.: Comparative evaluation of dynamic performance of a virtual synchronous machine and synchronous machines. IET Conf. Publ. 2021(CP783), 366–371 (2021). https://doi.org/10.1049/ICP.2021.1362/CITE/REFWORKS
21. Yu, M., et al.: Instantaneous penetration level limits of nonsynchronous devices in the British power system. IET Renew. Power Gener. 11(8), 1211–1217 (2017). https://doi.org/10.1049/iet-rpg.2016.0352.
22. Triphase: Programmable Power Converters and Measurements for PHIL and Power Systems Prototyping. Heverlee, Belgium (2016). https://www.rikei.co.jp/wp/wp-content/uploads/2017/10/Triphase.pdf

How to cite this article: Khan, M.A.U., Hong, Q., Liu, D., Egea-Àlvarez, A., Avras, A., Dyśko, A., Booth, C., Rostom, D.: Experimental assessment and validation of inertial behaviour of virtual synchronous machines. IET Renew. Power Gener. 1–11 (2022). https://doi.org/10.1049/rpg2.12496